

Activating calcium-sensing receptor mutation in the mouse is associated with cataracts and ectopic calcification

Tertius A. Hough*, Debora Bogani*, Michael T. Cheeseman*, Jack Favor†, M. Andrew Nesbit‡, Rajesh V. Thakker‡, and Mary F. Lyon*[§]

*Mammalian Genetics Unit and Mary Lyon Centre, Medical Research Council, Harwell, Oxfordshire OX11 0RD, United Kingdom; †GSF-National Research Center for Environment and Health, Institute of Human Genetics, D-85764 Neuherberg, Germany; and ‡Academic Endocrine Unit, Nuffield Department of Clinical Medicine, Oxford Centre for Diabetes, Endocrinology, and Metabolism, University of Oxford, Churchill Hospital, Headington, Oxford OX3 7LJ, United Kingdom

Contributed by Mary F. Lyon, August 4, 2004

The extracellular calcium-sensing receptor (CaSR) plays a pivotal role in the regulation of extracellular calcium such that abnormalities, which result in a loss or gain of function, lead to hypercalcemia or hypocalcemia, respectively, in patients. Mice carrying CaSR knockout alleles develop hypercalcemia that mimics the disorders observed in humans. To date, there is no mouse model for an activating CaSR mutation. Here, we describe such a mouse model, named *Nuf*, originally identified for having opaque flecks in the nucleus of the lens in a screen for eye mutants. *Nuf* mice also display ectopic calcification, hypocalcemia, hyperphosphatemia, and inappropriately reduced levels of plasma parathyroid hormone. These features are similar to those observed in patients with autosomal dominant hypocalcemia. Inheritance studies of *Nuf* mice revealed that the trait was transmitted in an autosomal-dominant manner, and mapping studies located the locus to chromosome 16, in the vicinity of the CaSR gene (Mouse Genome Database symbol *Gprc2a*). DNA sequence analysis revealed the presence of a *Gprc2a* missense mutation, Leu723Gln. Transient expression of wild-type and mutant CaSRs in human embryonic kidney 293 cells demonstrated that the mutation resulted in a gain of function of the CaSR, which had a significantly lower EC₅₀. Thus, our results have identified a mouse model for an activating CaSR mutation, and the development of ectopic calcification and cataract formation, which tended to be milder in the heterozygote *Nuf* mice, indicates that an evaluation for such abnormalities in autosomal dominant hypocalcemia patients who have activating CaSR mutations is required.

The extracellular calcium-sensing receptor (CaSR) Online Mendelian Inheritance in Man (OMIM) accession no. 601199 is a plasma membrane-bound protein that is predominantly expressed in the parathyroids and kidneys, where it regulates parathyroid hormone (PTH) secretion and renal tubular calcium reabsorption appropriate to the prevailing extracellular calcium concentration ($[Ca^{2+}]_o$) (1–4). The CaSR is also expressed in other tissues that include the thyroid, intestine, bone, bone marrow, brain, skin, lens epithelium, pancreas, lung, and heart, where its function remains to be defined (1). The CaSR is a member of family C of the superfamily of G protein-coupled receptors that includes the metabotropic glutamate receptors, some pheromone receptors, and the γ -amino butyric acid receptors (1, 5). Ligand binding by the CaSR results in G protein-dependent stimulation, mediated by Gq/11, of phospholipase C activity causing an accumulation of inositol 1,4,5-trisphosphate and rapid release of calcium ions from intracellular stores. This release is followed by an influx of extracellular calcium ions (1–3). The increase in intracellular calcium results in activation of phosphokinase C, which in turn activates the mitogen-activated protein kinase (MAPK) pathway (1, 6). The CaSR can also activate the MAPK pathway through an isoform of Gi that inhibits adenylate cyclase and that activates Src-family tyrosine kinases (1, 6). The manner in which these intracellular

events regulate parathyroid cell proliferation and the rate of PTH secretion from the parathyroid cell, together with the reduction in renal tubular calcium reabsorption, remains to be elucidated. However, much has been learned about the role of the CaSR in the regulation of extracellular calcium homeostasis by the identification of CaSR mutations in human disorders (www.casrdb.mcgill.ca) and by studies of CaSR knockout mice (7). In man, inactivating CaSR mutations result in familial (benign) hypocalciuric hypercalcemia (FBHH), OMIM accession no. 145980, and neonatal severe primary hyperparathyroidism (NSHPT), OMIM accession no. 239200 (8, 9), whereas activating CaSR mutations result in autosomal dominant hypocalcemia (ADH), OMIM accession no. 601198 (10, 11), which may be sometimes associated with hypercalciuria and a Bartter-like syndrome (12, 13). Furthermore, mice heterozygous for a CaSR knockout allele mimic the phenotype of FBHH patients with modest elevations in serum calcium and relative hypocalciuria, whereas homozygous mice exhibit a phenotype similar to NSHPT, with severe hypercalcemia, parathyroid hyperplasia, bone abnormalities, and neonatal death (14). The understanding of the manner in which the CaSR exerts these effects would be greatly enhanced by the availability of a mouse model with an activating CaSR mutation. Here, we describe such a model that bears the mutation *Gprc2a*^{*Nuf*} (which will be referred to as *Nuf*). The founder animal was identified by screening mouse mutants that were generated by use of the mutagenic alkylating chemical, isopropyl methane sulfonate (15, 16).

Materials and Methods

Experimental Animals. All studies were performed under the guidance issued by the Medical Research Council and Home Office Project license nos. 30/1517 and 30/2049. Mouse lines were housed on site in a controlled environment and were sustained on expanded rat and mouse no. 3 breeding diet (Special Diets Services, Witham, Essex, U.K.) containing 1.15% calcium, 0.82% total phosphorus, and 4088.68 units/kg vitamin D.

Generation of Mutant Mice. The original mutant animal, known as iPMS-112, was found in a mutagenesis experiment at the Institute of Mammalian Genetics (Neuherberg, Germany), in which males of genotype (C3H/He × 102/EI)/F1/(the 102 stock is thought to have arisen from a cross of strain 101 with C3H) were

Abbreviations: CaSR, calcium-sensing receptor; PTH, parathyroid hormone; ADH, autosomal dominant hypocalcemia; HEK, human embryonic kidney; $[Ca^{2+}]_o$, extracellular calcium concentration; $[Ca^{2+}]_i$, intracellular calcium concentration; EGFP, enhanced GFP.

[§]To whom correspondence should be addressed at: Medical Research Council Mammalian Genetics Unit, Harwell, Didcot, Oxfordshire OX11 0RD, United Kingdom. E-mail: m.lyon@har.mrc.ac.uk.

© 2004 by The National Academy of Sciences of the USA

treated with isopropyl methane sulfonate and bred so that spermatogonial stem cells were sampled. The offspring were scored for cataracts (16). The animal iPMS-112 had “nuclear flecks” in the lens. When crossed with a normal mouse, it produced offspring with a similar phenotype, indicating autosomal dominant inheritance. The mutant was transferred to Medical Research Council Harwell (Oxfordshire, U.K.) for further studies and given the name “nuclear flecks” and symbol *Nuf*.

Phenotype Screen. Mice aged 4–6 weeks were phenotyped for presence of opaque flecks in the lens nucleus by slit lamp biomicroscopy (Zeiss 30SL/M) at $\times 20$ magnification with a narrow beam slit lamp illumination at a 25–30° angle from the direction of observation. Dilation of the pupil was achieved with 1% atropine sulfate (Schering-Plough) applied at least 10 min before examination.

Animals for Further Studies. Animals for histology and biochemistry were obtained from a homozygous breeding stock of *Nuf/Nuf* with a background of strains C3H and 102. For normal controls the inbred strain 102/H was used and heterozygous *Nuf/+* animals were obtained by crossing *Nuf/Nuf* \times 102/H.

Mapping. *Nuf/+* mice were crossed to C57BL/6 and affected offspring were backcrossed to C3H/HeH. Backcross offspring were scored for cataract and were then typed for microsatellite markers spaced at ≈ 20 -cM intervals throughout the genome, which can be accessed at www.informatics.jax.org. DNA was extracted from tail tissues by using Nucleon Biosciences genomic DNA extraction kits (Amersham Biosciences, Piscataway, NJ) (Nucleon HT protocol for hard tissues). Any areas of potential linkage were expanded by the inclusion of additional markers in that region. PCR conditions were described (17).

Biochemical Analysis. All samples were collected from mice that were allowed to eat and drink ad libitum. Samples were not collected from breeding pairs or lactating females. Blood samples were collected from the lateral tail vein from groups of mice (age ≈ 120 days, $n = 7$ –10 for each sex and genotype) as described (18). Urine samples (from the same cohorts) were collected into Eppendorf tubes and frozen at -70°C until analysis. Plasma and urine samples were analyzed for calcium, phosphate, creatinine, sodium, potassium, chloride, magnesium, and bicarbonate by using an Abbott Aeroset analyzer. Urine parameters were calculated relative to sample creatinine. Plasma PTH concentration was measured (age ≈ 90 days, $n = 4$ –5 for each cohort) by using a commercial ELISA specific for mouse intact PTH (Immutopics, San Clemente, CA) with a detection limit of 0.5 pmol/liter. All statistical analyses were performed in Microsoft Excel.

Pathology. Male and female *Nuf/Nuf*, *Nuf/+*, and 102/H controls (age range 116–430 days) were examined by gross post mortem and histology. The primary objective was to evaluate the extent of ectopic mineralization and to determine parathyroid tissue status in *Nuf/Nuf* and *Nuf/+* mice. Mice were killed by a barbiturate overdose administered i.p. The lungs were inflated with 10% neutral buffered formalin (NBF), leaving the heart attached to avoid accidental lung puncture. All tissues were fixed in 10% NBF with the exception of testes that were fixed in Bouin's solution and the eyes in Davidson's solution. Bony tissues were decalcified in 10% formic acid. After decalcification, cross and longitudinal sections of lumbar vertebral column and three cross sections of snout were cut. The remainder of the head was embedded and sectioned in dorsal plane to examine the middle ear. The brain was fixed for 48 h in NBF and four coronal slices were cut at the level of the rostral olfactory cortex, thalamus, midbrain, and cerebellum/brainstem. After process-

ing to wax, 4- μm sections were cut and stained with hematoxylin/eosin. Selected sections were stained by Von Kossa's method for calcium. Faxitron digital x-ray images of selected NBF-fixed tongues were made to assess the macroscopic pattern of soft tissue mineralization before histological processing.

DNA Sequence Analysis. DNA was extracted from mouse kidney by using a Puregene DNA isolation kit (Gentra Systems). Fourteen pairs of primers (details available on request) were used for the PCR amplification of the seven exons and 12 intron-exon boundaries of *Gprc2a* (the mouse orthologue of the human CaSR). The DNA sequences of both strands were determined as described (19) and were resolved on a semiautomated 377 sequencer detection system (Applied Biosystems). DNA sequence abnormalities in the *Nuf* mice were confirmed by *Pst*I restriction endonuclease analysis (New England Biolabs) as described (11).

Functional Expression of CaSR. Functional studies were performed by using a human CaSR cDNA construct (20) because the human and mouse CaSR amino acid sequences are 92% identical and are 100% identical in the region surrounding the mutated site. The reported pcDNA3-CaSR construct (11) was subcloned into the pEGFP-N2 vector (BD Biosciences Clontech, Palo Alto, CA) and the Q723 mutation was introduced by site-directed mutagenesis (QuikChange, Stratagene) as reported (21). The wild-type and mutant CaSRs were transiently transfected into human embryonic kidney (HEK)293 cells (American Type Culture Collection catalog no. CRL1573) by using Lipofectamine Plus (Invitrogen) as described (20). Cells were visualized by using a Nikon Eclipse E400 microscope with a Y-FL Epifluorescence attachment and a triband 4',6-diamidino-2-phenylindole-FITC-Rhodamine filter, as reported (21). Expression of CaSR-EGFP fusion proteins was also confirmed by Western blot analysis of cellular protein extracts using an antibody to GFP (Santa Cruz Biotechnology) as reported (21).

The wild-type and mutant CaSRs were functionally assessed by measuring the alterations in intracellular calcium concentration ($[\text{Ca}^{2+}]_i$) in response to changes in $[\text{Ca}^{2+}]_o$ as follows. Forty-eight hours posttransfection, the cells were harvested, washed twice in Ca- and Mg-free Hanks' balanced salt solution (HBSS) (Invitrogen), and loaded with 1 $\mu\text{g}/\text{ml}$ indo-1 acetoxymethyl ester (Molecular Probes) for 1 h at 37°C . After removal of free dye by centrifugation and washing with Ca- and Mg-free HBSS, the cells were resuspended in 1 ml of Ca- and Mg-free HBSS and maintained at 37°C . Flow-assisted cell sorting was performed with a Cytomation MoFlo flow cytometer (Dako-Cytomation, Carpinteria, CA) equipped with an argon laser (Coherent Radiation, Palo Alto, CA) as described (22, 23). Baseline fluorescence ratio was measured for 2 min, the fluorescence ratio versus time was recorded, and data were collected for 2 min at each $[\text{Ca}^{2+}]_o$. Cytomation SUMMIT software was used to determine the peak mean fluorescence ratio of the transient response after each individual stimulus and normalized response. $[\text{Ca}^{2+}]_o$ curves were generated as described (20). EC_{50} (i.e., $[\text{Ca}^{2+}]_o$ required for 50% of the maximal response) for each normalized concentration-response curve was determined, and the mean EC_{50} for six separate transfection experiments was used for statistical comparison by using Student's *t* test.

Results

The founder animal was identified by having opaque flecks in the nucleus of the eye lens in a screen for new eye mutants. Subsequent histological and biochemical investigations revealed that the cataracts constituted only a minor part of the phenotype, which also included ectopic calcification, hypocalcemia, hyperphosphatemia, inappropriately reduced levels of plasma PTH, and sudden death.

Table 1. Inheritance of cataracts among offspring of heterozygotes and homozygotes for *Nuf* mice

Genotype of parents	Offspring		Percent with cataract	χ^2	<i>P</i>
	Cataract	Normal			
<i>Nuf/+</i> × <i>+/+</i>	65	61	51.6	0.127	>0.7
<i>Nuf/+</i> × <i>Nuf/+</i>	79	44	64.2	7.61	<0.01
<i>Nuf/+</i> ? × <i>+/+</i>	70	96	42.2	4.07	<0.05
<i>Nuf/Nuf</i> × <i>+/+</i>	52	0	100	—	—
<i>Nuf/Nuf</i> × <i>Nuf/Nuf</i>	31	0	100	—	—

Inheritance Studies. In all of the breeding studies, the phenotype of the animals was determined by slit lamp examination for cataracts. *Nuf/+* heterozygotes were crossed with normal C3H/HeH or 102/H control animals, and crosses of *Nuf/+* × *Nuf/+* were made to detect homozygous *Nuf/Nuf* (Table 1). The cataract phenotype of heterozygotes was very mild (Fig. 1*B*) and classification as normal or affected was difficult. A few mice scored as affected bred as if in fact normal. It is reasonable to suppose that also a few *Nuf/+* mice were wrongly scored as normal. Among the offspring of *Nuf/+* × *Nuf/+*, some animals were more severely affected, suggesting that they might be homozygotes. This result was confirmed by crosses of affected offspring of intercrosses to normal to detect those that produced affected young only. Of 21 young tested, 2 bred as *Nuf/Nuf* and 2 of 7 young of *Nuf/Nuf* × *Nuf/+* also bred as *Nuf/Nuf*. From these mice, a homozygous breeding stock of *Nuf/Nuf* was set up. The cataracts of the *Nuf/Nuf* mice were in general more severe than those of *Nuf/+*, but there was overlap in severity of phenotype, and it was not possible to score animals as *Nuf/Nuf* or *Nuf/+* by cataract phenotype alone (Fig. 1*A–C*). The ratio of affected to normal young among offspring of *Nuf/+* × *Nuf/+* was significantly <3:1 ($\chi^2 = 7.61$, *df* = 1, *P* < 0.01) and the proportion of affected offspring that bred as *Nuf/Nuf* was also less than the expected one-third, although not significantly so. Possible explanations for this result include misclassification of *Nuf/+* young as *+/+* and *Nuf/Nuf* young as *Nuf/+*, or the death of some *Nuf/Nuf* before classification.

The cataracts consisted of a group of small opaque dots in the lens nucleus. In homozygotes, the dots were larger and more numerous than in heterozygotes (Fig. 1*A–C*). The cataracts were present at 4–6 weeks of age. Some animals were observed up to ≈1 year of age and the cataracts did not appear to increase in severity. However, in homozygotes, scattered corneal opacities were evident at later ages and these appeared to worsen.

A proportion of *Nuf/Nuf* breeding mice, mainly lactating females, died suddenly. In one 12-month period, of a total of 31 mated females and 16 males, 15 females and 4 males were found dead. At the time of death, 11 females were lactating with their first to third litters. Over the same time period, and in the same animal room, 11 pairs of the 102/H control strain, and 16 females and 8 males of a different cataract strain were mated and no deaths were observed. The affected *Nuf/Nuf* animals appeared healthy and were found dead the next day, without any intervening illness. At necropsy, no gross abnormalities were seen, but on histological analysis, foci of calcification were observed in various tissues.

Biochemical Phenotypes. The male and female *Nuf/+* and *Nuf/Nuf* mice had significant hypocalcemia and hyperphosphatemia that was associated with inappropriately reduced plasma PTH levels (Table 2). No significant differences were observed in plasma and urinary magnesium. Normal plasma magnesium in the mutant mice indicated that hypomagnesemia was not a secondary cause for impaired PTH secretion. The

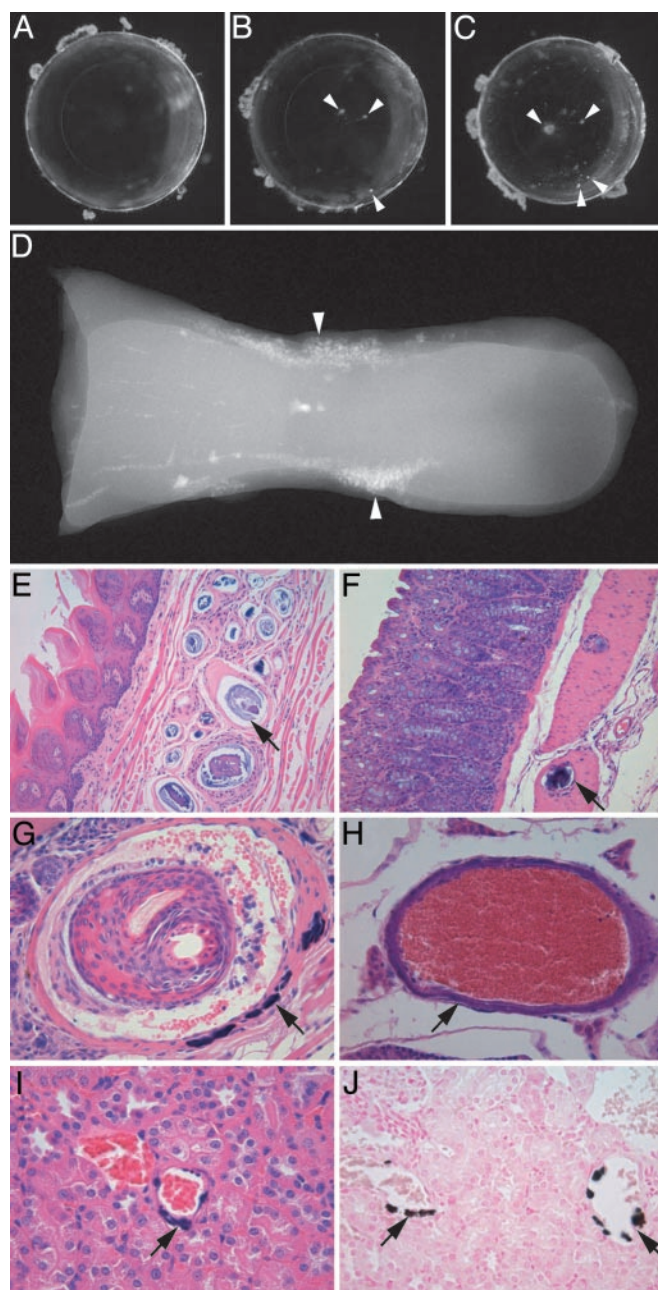


Fig. 1. Ectopic calcification and cataract formation in *Nuf* mice. (*A–C*) Cataracts in lenses (arrowheads). (*A*) Normal control 102/H mice. (*B*) *Nuf/+* mice with few nuclear flecks. (*C*) *Nuf/Nuf* mice with more and larger flecks. (*D–J*) Soft tissue mineralization in *Nuf/Nuf* mutants. Arrows indicate sites of mineralization. (*D*) Faxitron x-ray image of a fixed tongue. (*E–J*) Hematoxylin/eosin-stained sections original magnification ×200 of the tongue (*E*), colon (*F*), skin vibrissa dermal sheath (*G*), testis artery wall (*H*), and blood vessels (*I*) in kidney cortex. (*J*) Positive Von Kossa staining confirms a calcium component of the mineralized deposits in the renal blood vessels.

Nuf/+ and *Nuf/Nuf* mice did not have significantly elevated urinary excretion of calcium and phosphate, although the *Nuf/Nuf* females were hypocalciuric and both *Nuf/Nuf* males and females were hypophosphaturic (Table 2). Additional biochemical data for plasma bicarbonate and plasma and urinary sodium, potassium and chloride is provided in Table 4, which is published as supporting information on the PNAS web site.

Table 2. Plasma and urine biochemical profiles of 102/H control, *Nuf/+*, and *Nuf/Nuf* mice (means \pm 1 SD)

Genotype	Female			Male		
	102/H control	<i>Nuf/+</i>	<i>Nuf/Nuf</i>	102/H control	<i>Nuf/+</i>	<i>Nuf/Nuf</i>
Plasma calcium (mmol/liter)	2.53 \pm 0.12	1.82 \pm 0.03 [†]	1.55 \pm 0.13 ^{†¶}	2.34 \pm 0.05	1.78 \pm 0.17 [†]	1.48 \pm 0.13 ^{†¶}
Plasma phosphate (mmol/liter)	1.43 \pm 0.29	2.86 \pm 0.19 [†]	3.39 \pm 0.72 [†]	1.72 \pm 0.13	3.26 \pm 0.42 [†]	3.93 \pm 1.06 [†]
Plasma creatinine (μ mol/liter)	45 \pm 9.81	41 \pm 4.78	42 \pm 10.80	36 \pm 1.46	37 \pm 2.32	40 \pm 2.75 ^{†¶}
Plasma magnesium (mmol/liter)	0.64 \pm 0.07	0.67 \pm 0.21	0.60 \pm 0.10	0.52 \pm 0.03	0.47 \pm 0.07	0.51 \pm 0.06
Plasma PTH (pmol/liter)	3.4 \pm 2.07	1.0 \pm 0.59 [*]	0.3 \pm 0.22 ^{*†}	3.4 \pm 1.73	0.5 \pm 0.21 [†]	0.6 \pm 0.10 [†]
Urine calcium/creatinine ratio	0.3 \pm 0.20	0.2 \pm 0.05	0.1 \pm 0.04 [*]	0.2 \pm 0.07	0.2 \pm 0.08	0.2 \pm 0.08
Urine phosphate/creatinine ratio	12.7 \pm 4.40	11.2 \pm 2.37	8.0 \pm 2.61 [*]	10.3 \pm 3.59	9.5 \pm 1.30	5.9 \pm 2.02 [†]
Urine magnesium/creatinine ratio	3.1 \pm 0.30	3.1 \pm 0.52	2.5 \pm 0.34 [†]	2.8 \pm 0.44	2.9 \pm 0.30	2.7 \pm 0.40

^{*}, $P = 5 \times 10^{-2}$ to 5×10^{-3} . [†], $P < 5 \times 10^{-3}$ for Student's *t* test, respectively, comparing *Nuf/+* and *Nuf/Nuf* mice with same-sex 102/H controls. [‡], $P = 5 \times 10^{-2}$ to 5×10^{-3} . [¶], $P < 5 \times 10^{-3}$ for Student's *t* test comparing *Nuf/Nuf* with same-sex *Nuf/+* mice.

Pathology Phenotypes. Homozygous *Nuf/Nuf* mice had small scattered mineralized foci (without ossification), particularly in the tongue and other striated muscle, vibrissa dermal sheath, visceral smooth muscle, and blood vessels. Mineralization at these sites was much less evident in the *Nuf/+* heterozygotes and was not seen in 102/H controls (Table 3). Although the mice of different genotypes were not precisely age-matched, the age range in each group overlapped. Mineralization was seen consistently in the youngest *Nuf/Nuf* mice examined at \approx 130 days

and, with the exception of the reproductive tract, heart, and kidney tubules, there was no comparable mineralization in *Nuf/+* mice up to \approx 350 days old. In comparison with another inbred strain, C3H, that is predisposed to soft tissue mineralization, the incidence of mineralization at the two most common sites in *Nuf/Nuf* mice, the vibrissa dermal sheath (88%) and tongue (97%), was more than twice that in a similar aged group of C3H mice (33% and 40%, respectively). In the tongue, mineralization was accompanied by localized histiocytic reaction, but in other tissues there was no localized inflammatory reaction. The clinical significance of vascular mineralization is uncertain, but there was no evidence of ischemic injury to the tissues that the blood vessels supply.

Table 3. Sites of ectopic mineralization in male and female *Nuf/Nuf*, *Nuf/+*, and 102/H control mice

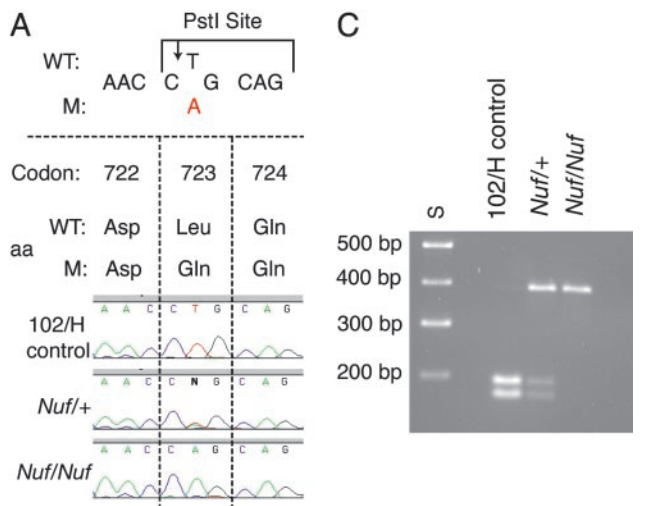
Sites of ectopic calcification	<i>Nuf/Nuf</i>	<i>Nuf/+</i>	102/H
Striated muscle			
Tongue	28/32 (88)	0/16 (0)	0/11 (0)
Jaws	20/26 (77)	0/16 (0)	0/11 (0)
Axial and appendicular skeleton	16/24 (67)	0/16 (0)	0/11 (0)
Kidneys			
Arcuate and interlobular arteries	18/32 (56)	0/16 (0)	0/11 (0)
Hilar artery	12/32 (38)	0/16 (0)	0/11 (0)
Cortical capillaries	14/32 (44)	1/16 (6)	0/11 (0)
Cortical tubules	25/32 (78)	8/16 (50)	1/11 (9)
Papillary tubules	13/32 (41)	10/16 (63)	1/11 (9)
Vibrissa dermal sheath	31/32 (97)	0/16 (0)	0/11 (0)
Heart myocytes	17/32 (53)	11/16 (69)	2/11 (18)
Aorta, elastic, and muscular arteries	12/32 (38)	0/16 (0)	1/11 (9)
Choroid and meninges	15/32 (47)	0/16 (0)	0/11 (0)
Stomach	3/32 (9)	0/16 (0)	0/11 (0)
Small intestine muscle and serosa	15/32 (47)	0/16 (0)	0/11 (0)
Large intestine muscle and serosa	19/32 (59)	0/16 (0)	0/11 (0)
Brown fat	8/24 (33)	0/16 (0)	0/11 (0)
Lung alveolus septa	12/32 (38)	0/16 (0)	0/11 (0)
Testis artery	8/9 (89)	1/9 (11)	0/5 (0)
Male accessory glands	4/9 (44)	4/9 (44)	0/5 (0)
Uterus artery	1/23 (4)	0/7 (0)	0/6 (0)
Ovary stroma	7/23 (30)	1/7 (14)	1/6 (17)

Data in the body of the table are reported as positive cases/number of mice examined and percent positive in parentheses. Less frequent sites of ectopic mineralization include eye retinal pigmented epithelium and cornea, ear spiral ganglion, and trigeminal ganglion. The pituitary, thyroids, and parathyroids, trachea, pancreas, liver, adrenals, spleen, sciatic nerve, skin samples from the dorsum and ventrum, lumbar vertebral column, knee joint, tail, foot, and middle ears were also examined but were not found to be sites of ectopic calcification. Ocular findings included small foci of corneal mineralization in *Nuf/Nuf* mice and cataracts (see text for details). The numbers of mice examined, their age range, and ages of individual mice are provided separately in Data Set 1, which is published as supporting information on the PNAS web site.

Micronodular soft tissue mineralization was evident in x-ray images in the midlateral regions of the tongue (Fig. 1D), and this result corresponded to basophilic concretions in hematoxylin/eosin sections (Fig. 1E). The calcium component of larger mineralized concretions in the tongue and intestine smooth muscle (Fig. 1F) was confirmed by Von Kossa's staining (data not shown), but in small deposits in the vibrissa dermal sheath (Fig. 1G), Von Kossa's staining was weak or absent. Vascular mineralization is common in testis artery and renal artery and capillaries (Fig. 1H–J). The ocular pathology findings confirmed that the nuclear flecks in *Nuf/Nuf* mice were small cataracts comprised of foci of lens fiber swelling and degeneration without a significant degree of mineralization. In a few cases, there were also small foci of corneal mineralization (data not shown). Serial cross sections of the thyroids of selected *Nuf/Nuf* mice confirmed histologically normal bilateral parathyroids were present in all cases. Single sections confirmed the presence of parathyroid tissue in other cases.

Chromosomal Localization of *Nuf* Locus. Preliminary results by using informative markers showed significant linkage of the phenotype to *D16Mit131* ($\chi^2 = 8.26$, $df = 1$, $P < 0.01$; data not shown). The same sets of animals were then typed with further chromosome 16 markers. Some animals gave anomalous results, suggesting that they were misclassified for *Nuf* and these results were excluded. Results from the remaining 53 mice indicated that the *Nuf* locus lies distal to *D16Mit88* and proximal to markers *D16Mit103* and *D16Mit134*. The recombination percentages were *D16Mit131*–3.8 \pm 2.6–*D16Mit88*–7.6 \pm 3.6–*Nuf*–7.6 \pm 3.6–(*D16Mit103*, *D16Mit134*)–3.8 \pm 2.6–*D16Mit88*–1.9 \pm 1.9–*D16Mit173*–7.6 \pm 3.6–*D16Mit189*. This result placed the *Nuf* locus near position 18 cM, thus making *Gprc2a* (coding for the CaSR) a candidate gene.

Identification of the Mutation in *Gprc2a* (the Mouse CaSR) and Its Functional Characterization. Analysis of the DNA sequence of the entire 3,234-bp coding region and of the 810 bp of the two 5'-noncoding exons of *Gprc2a* revealed a homozygous missense



B

Species	Position	Sequence	Residue
<i>Nuf/Nuf</i>	712	T S F H R K W W G L N Q Q F L L V F L C T F M	Gln
<i>Mus musculus</i>	712	T S F H R K W W G L N L Q F L L V F L C T F M	Leu
<i>Rattus norvegicus</i>	712	T S F H R K W W G L N L Q F L L V F L C T F M	Leu
<i>Homo sapiens</i>	712	T S F H R K W W G L N L Q F L L V F L C T F M	Leu
<i>Bos taurus</i>	713	T S F H R K W W G L N L Q F L L V F L C T F M	Leu
<i>Squalus acanthius</i>	720	T S L H R K W W G L N L Q F L L V F L C I L V	Leu
<i>Sparus aurata</i>	697	T S L H R K W W G L N L Q F L L V F L C T F V	Leu
<i>Takifugu rubripes</i>	690	T S I H R K W W G L N L Q F L L V F L C T F V	Leu

Fig. 2. Missense mutation in exon 7 of the CaSR (*Gprc2a*) of the *Nuf* mouse. (A) Analysis of the DNA sequence revealed an A-to-T transversion at codon 723 in the *Nuf/Nuf* mice. (B) At codon 723, the wild-type (WT) sequence is CTG encoding an evolutionarily conserved (arrowed) Leu (L) residue, whereas the mutant (M) sequence is CAG encoding a Gln (Q) residue. (C) The missense mutation resulted in the loss of a *PstI* restriction enzyme site (CTGCA/G) and this mutation facilitated its confirmation. Amplification with PCR and digestion with *PstI* resulted in two products of 179 and 172 bp, respectively, from the 102/H control sequence, but a larger product of 351 bp from the mutant sequence. S, DNA size marker (100-bp ladder).

mutation in the fourth transmembrane domain of the receptor in the *Nuf/Nuf* mice (Fig. 2A). This mutation, which consisted of a T-to-A transversion (CTG to CAG) at codon 723, predicted the substitution of an evolutionary conserved Leu (L) by a Gln (Q) residue (Fig. 2B). The mutation was associated with the loss of a *PstI* restriction enzyme site, which facilitated its detection (Fig. 2C). *Nuf/Nuf* mice were homozygous for the Q723 mutation, *Nuf/+* mice were heterozygous (L/Q723), and control 102/H mice were homozygous for L723. Functional expression of the wild-type and mutant CaSRs was undertaken by using HEK293 cells (Fig. 3). The mutant and wild-type CaSR were both expressed mainly at the plasma membrane and in the cytoplasm but not in the nucleus (Fig. 3A–C). Western blot analysis confirmed expression of the mutant and wild-type CaSRs as 167-kDa proteins (Fig. 3D), which consisted of the 140-kDa CaSR tagged with a 27-kDa enhanced GFP (EGFP). A functional characterization of the wild-type and mutant CaSRs, as assessed by the alteration in $[Ca^{2+}]_i$ in response to $[Ca^{2+}]_o$, revealed the mutant CaSR to have a significantly ($P < 0.01$) lower EC_{50} ($1.95 \text{ mM} \pm 0.12$) when compared with the EC_{50} of the wild type (2.25 ± 0.07) (Fig. 3E). Thus, the mutant CaSR showed a significant leftward shift in its concentration–response curve when compared with the wild type, thereby demonstrating that the mutant CaSR is active at a lower $[Ca^{2+}]_o$ than the wild

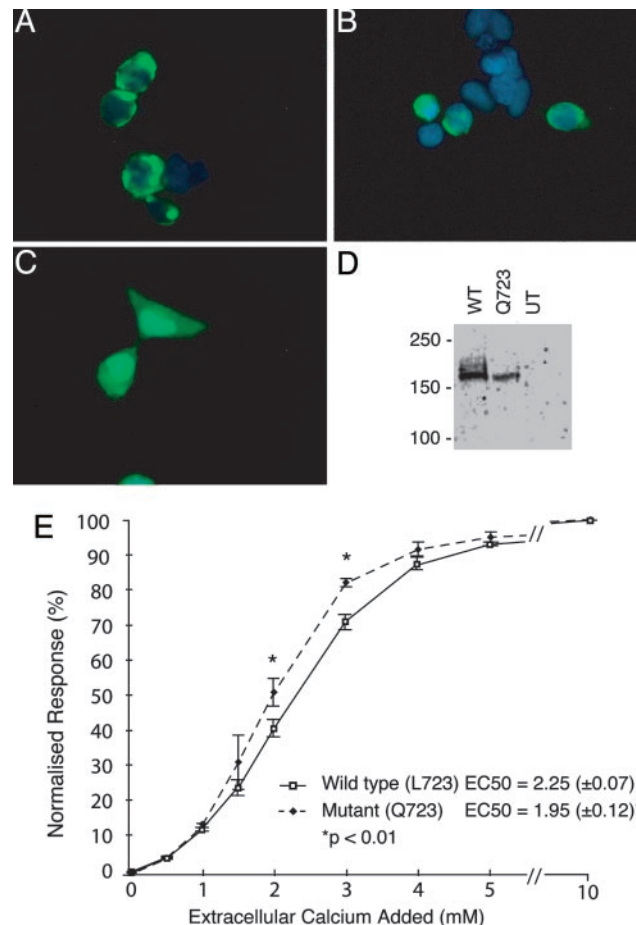


Fig. 3. Functional expression in HEK293 cells of the wild-type (WT) (L723) and mutant (Q723) CaSRs. HEK293 cells were transiently transfected with wild-type or the mutant CaSR-EGFP construct or with empty EGFP vector. Fluorescence microscopy was used to confirm successful transfection. (A and B) HEK293 cells transfected with wild-type (A) or mutant (B) CaSR showed similar expression patterns with fluorescence in the cytoplasm and at the plasma membrane, but not in the nucleus. (C) Cells transfected with pEGFP alone showed a uniform, nonspecific fluorescence pattern, whereas untransfected cells had no fluorescence (data not shown). The cells were counterstained with 4',6-diamidino-2-phenylindole to show the nuclei (blue). (D) Western blot analysis of total cell protein extracts from HEK293 cells (transfected with either wild-type or the mutant CaSR by using an anti-GFP antibody) confirmed the expression of EGFP-tagged CaSRs (167 kDa), which was not present in untransfected (UT) cells. (E) Single, live cells loaded with indo-1 acetoxymethyl ester, emitting fluorescence at 525 nm, and hence containing transfected CaSR were selected by fluorescence-activated cell sorting and the $[Ca^{2+}]_o$ -evoked increases in $[Ca^{2+}]_i$ were measured. The increments in $[Ca^{2+}]_o$ from 0 to 10 mM are shown on the x axis, and the $[Ca^{2+}]_i$ response, which was measured as a percentage of the maximum normalized response, is shown on the y axis (mean \pm SD of six estimations). The EC_{50} of the mutant CaSR was significantly lower ($P < 0.01$) than that of the wild-type CaSR. The lower EC_{50} and the leftward shift of the concentration–response curve of the mutant CaSR indicate that this mutation confers a gain of function of the mutant CaSR.

type, which is consistent with it being an activating mutation of the *Gprc2a* gene.

Discussion

Our studies have identified a mutant mouse line (*Nuf*) with an activating CaSR mutation that results in hypocalcemia, hyperphosphatemia, cataracts, and ectopic calcification (Fig. 1). The data provide strong evidence that the mutation in the mouse CaSR gene (*Gprc2a*) underlies the observed phenotypic effects.

The amino acid substitution observed in the *Nuf* mice is unlikely to be a silent polymorphism, because the leucine residue altered is highly conserved among species (Fig. 2). The alteration from a leucine residue, which is nonpolar and hydrophobic, to a polar and hydrophilic glutamine residue, leads to a functional change as demonstrated by the transient transfection experiments in which cells transfected with a *Nuf* mutant CaSR show an increase in sensitivity to calcium ions, as expected for an activating mutation (Fig. 3). Certain phenotypic abnormalities were more pronounced in *Nuf/Nuf* mice than in *Nuf/+* mice, which suggests a dosage effect of the mutated allele. However, this result was not the case for all of the parameters investigated.

Nuf/+ mice have similarities to ADH patients with heterozygous activating CaSR mutations, including hypocalcemia, hyperphosphatemia, and inappropriately low plasma PTH concentrations (Table 2 and ref. 11). However, there are also important differences. The *Nuf/+* and *Nuf/Nuf* mice are not hypercalciuric, whereas patients with activating CaSR mutations have an elevated urinary calcium excretion that increases with vitamin D supplementation (1, 11, 24). The vitamin D content of the diet (24, 25) may not have been sufficient to render the *Nuf/+* and *Nuf/Nuf* mice hypercalciuric. Additional studies of these mice by using metabolic cages for 24-h urine collection, which are more reliable than the spot collections used in the present study (11), are required to further characterize the effects of the Q723 mutation in the CaSR on the renal handling of calcium and phosphate.

The *Nuf/+* and *Nuf/Nuf* mice developed cataracts and a heightened incidence of ectopic calcification at all of the common noncardiac sites reported in mice (26) (Table 3 and Fig. 1). Cataracts and ectopic calcification have not been reported in ADH patients with activating CaSR mutations. These features are milder in the heterozygous *Nuf/+* mice, and thus it is possible that in ADH patients, who are heterozygous for CaSR mutations, such mild abnormalities may not have been symptomatic and therefore may not have been detected. However,

soft tissue calcification has been reported in some ADH patients (11). For example renal calcification has been reported in >50% of ADH patients and basal ganglia calcification in 10%. The mechanisms underlying such calcifications are not known, but the identification of CaSR expression in the lens epithelial cells (27) and the finding that cataract formation is associated with elevated $[Ca^{2+}]_i$ (28) suggests a possible mechanism. Cataract formation is associated with elevated Ca^{2+} in the lens cells, and this elevated $[Ca^{2+}]_i$ triggers the activation of calpain, which in turn modifies the cytoskeletal proteins and a β -crystallin in lens cataract models (28, 29). Moreover, the lens possesses a large array of G protein receptors that are coupled to the release of Ca^{2+} (30, 31), including CaSR, which has been shown to be expressed in human lens epithelial cells (27). Thus, it is possible that the Q723 mutant CaSR of the *Nuf/+* and *Nuf/Nuf* mice results in activation at a lower $[Ca^{2+}]_o$ (Fig. 3), which in turn activates phospholipase C β that mobilizes inositol 1,4,5-trisphosphate and releases Ca^{2+} from intracellular stores. The rise in $[Ca^{2+}]_i$ will in turn activate calpain, which will lead to a modification of the cytoskeletal proteins that are known to be altered in lens cataracts models. This model for cataract formation, based on the observations of the activating CaSR mutation of the *Nuf* mice, may also apply to the occurrence of ectopic calcification at other sites where the CaSR is expressed. Our results on the *Nuf/+* and *Nuf/Nuf* mice also indicate that an evaluation for ectopic calcification and cataract formation in ADH patients is required.

We thank Nicola Chrobot, Gemma Frake, and Jim Humphreys for expert technical assistance; Bill Fraser for analysis of the PTH samples; Ian Draisey for analysis of plasma and urine samples; Nigel Rust for assistance with the measurement of intracellular calcium; and Asif Ali and Brian Harding for assistance with statistical analysis of data. This work was supported by the Medical Research Council and the Wellcome Trust (R.V.T.). T.A.H., D.B., M.T.C., M.A.N., and M.F.L. are supported by the Medical Research Council.

- Brown, E. M. & MacLeod, R. J. (2001) *Physiol. Rev.* **81**, 239–297.
- Brown, E. M. (1997) *Horm. Res.* **48**, 199–208.
- Hebert, S. C., Brown, E. M. & Harris, H. W. (1997) *J. Exp. Biol.* **200**, 295–302.
- Hofer, A. M. & Brown, E. M. (2003) *Nat. Rev. Mol. Cell Biol.* **4**, 530–538.
- Brown, E. M., Gamba, G., Riccardi, D., Lombardi, M., Butters, R., Kifor, O., Sun, A., Hediger, M. A., Lytton, J. & Hebert, S. C. (1993) *Nature* **366**, 575–580.
- Tfelt-Hansen, J., MacLeod, R. J., Chattopadhyay, N., Yano, S., Quinn, S., Ren, X., Terwilliger, E. F., Schwarz, P. & Brown, E. M. (2003) *Am. J. Physiol.* **285**, E329–E337.
- Ho, C., Conner, D. A., Pollak, M. R., Ladd, D. J., Kifor, O., Warren, H. B., Brown, E. M., Seidman, J. G. & Seidman, C. E. (1995) *Nat. Genet.* **11**, 389–394.
- Chou, Y. H., Brown, E. M., Levi, T., Crowe, G., Atkinson, A. B., Arnqvist, H. J., Toss, G., Fuleihan, G. E., Seidman, J. G. & Seidman, C. E. (1992) *Nat. Genet.* **1**, 295–300.
- Pollak, M. R., Brown, E. M., Chou, Y. H., Hebert, S. C., Marx, S. J., Steinmann, B., Levi, T., Seidman, C. E. & Seidman, J. G. (1993) *Cell* **75**, 1297–1303.
- Pollak, M. R., Brown, E. M., Estep, H. L., McLaine, P. N., Kifor, O., Park, J., Hebert, S. C., Seidman, C. E. & Seidman, J. G. (1994) *Nat. Genet.* **8**, 303–307.
- Pearce, S. H., Williamson, C., Kifor, O., Bai, M., Coulthard, M. G., Davies, M., Lewis-Barned, N., McCredie, D., Powell, H., Kendall-Taylor, P., et al. (1996) *N. Engl. J. Med.* **335**, 1115–1122.
- Vargas-Poussou, R., Huang, C., Hulín, P., Houillier, P., Jeunemaitre, X., Paillard, M., Planelles, G., Dechaux, M., Miller, R. T. & Antignac, C. (2002) *J. Am. Soc. Nephrol.* **13**, 2259–2266.
- Watanabe, S., Fukumoto, S., Chang, H., Takeuchi, Y., Hasegawa, Y., Okazaki, R., Chikatsu, N. & Fujita, T. (2002) *Lancet* **360**, 692–694.
- Kos, C. H., Karaplis, A. C., Peng, J. B., Hediger, M. A., Goltzman, D., Mohammad, K. S., Guise, T. A. & Pollak, M. R. (2003) *J. Clin. Invest.* **111**, 1021–1028.
- Ehling, U. H. & Neuhauser-Klaus, A. (1995) *Mutat. Res.* **328**, 73–82.
- Favor, J. & Neuhauser-Klaus, A. (2000) *Mamm. Genome* **11**, 520–525.
- Arkell, R. M., Cadman, M., Marsland, T., Southwell, A., Thaug, C., Davies, J. R., Clay, T., Beechey, C. V., Evans, E. P., Strivens, M. A., et al. (2001) *Mamm. Genome* **12**, 687–694.
- Hough, T. A., Nolan, P. M., Tsiouri, V., Toye, A. A., Gray, I. C., Goldsworthy, M., Moir, L., Cox, R. D., Clements, S., Glenister, P. H., et al. (2002) *Mamm. Genome* **13**, 595–602.
- Lloyd, S. E., Pearce, S. H., Fisher, S. E., Steinmeyer, K., Schwappach, B., Scheinman, S. J., Harding, B., Bolino, A., Devoto, M., Goodyer, P., et al. (1996) *Nature* **379**, 445–449.
- Pearce, S. H., Bai, M., Quinn, S. J., Kifor, O., Brown, E. M. & Thakker, R. V. (1996) *J. Clin. Invest.* **98**, 1860–1866.
- Nesbit, M. A., Bowl, M. R., Harding, B., Ali, A., Ayala, A., Crowe, C., Dobbie, A., Hampson, G., Holdaway, I., Levine, M. A., et al. (2004) *J. Biol. Chem.* **279**, 22624–22634.
- Carey, M. B. & Matsumoto, S. G. (2000) *Brain Res.* **862**, 201–210.
- Gergely, L., Cook, L. & Agnello, V. (1997) *Clin. Diagn. Lab. Immunol.* **4**, 70–74.
- Yamamoto, M., Akatsu, T., Nagase, T. & Ogata, E. (2000) *J. Clin. Endocrinol. Metab.* **85**, 4583–4591.
- Silva, I., Cebotaru, V., Wang, H., Wang, X., Wang, S., Guo, G., Devuyt, O., Thakker, R. V., Guggino, W. B. & Guggino, S. E. (2003) *J. Bone Miner. Res.* **18**, 619–623.
- Maronpot, R. R. (1999) *Pathology of the Mouse, Reference and Atlas* (Cache River Press, Vienna, IL).
- Chattopadhyay, N., Ye, C., Singh, D. P., Kifor, O., Vassilev, P. M., Shinohara, T., Chylack, L. T., Jr., & Brown, E. M. (1997) *Biochem. Biophys. Res. Commun.* **233**, 801–805.
- Churchill, G. C. & Louis, C. F. (2002) *Exp. Eye Res.* **75**, 77–85.
- Hejtmančík, J. F., Kaiser, M. I. & Piatigorsky, J. (2001) in *The Metabolic and Molecular Bases of Inherited Bone Diseases*, eds. Scriver, C. R., Beaudet, A. L., Sly, N. S., Valle, D., Childs, B., Kinzie, K. W. & Vogelstein, B. (McGraw-Hill, New York), Vol. 4, pp. 6033–6061.
- Duncan, G. & Collison, D. J. (2002) *Exp. Eye Res.* **75**, 377–389.
- Rhodes, J. D., Collison, D. J. & Duncan, G. (2003) *Invest. Ophthalmol. Visual Sci.* **44**, 3927–3932.